JTTEE5 13:361-369
DOI: 10.1361/10599630420371
1059-9630/$19.00 © ASM International

Characterization of Modified Thick Thermal Barrier Coatings

S. Ahmaniemi, J. Tuominen, M. Vippola, P. Vuoristo, T. Mäntylä, F. Cernuschi, C. Gualco, A. Bonadei, and R. Di Maggio

(Submitted October 6, 2003; in revised form October 31, 2003)

In gas turbines and diesel engines, there is a demand for thick thermal barrier coatings (TTBCs) due to the increased process combustion temperatures. Unfortunately, the increased thickness of plasma-sprayed thermal barrier coatings (TBCs) normally leads to a reduced coating lifetime. For that reason, the coating structures have to be modified. When modifying the structure of TTBCs, the focus is normally on elastic modulus reduction of the thick coating to improve the coating strain tolerance. On the other hand, coating structural modification procedures, such as sealing treatments, can be performed when increased hot-corrosion resistance or better mechanical properties are needed. In this article, several modified zirconia-based TTBC structures with specific microstructural properties are discussed. Coating surface sealing procedures such as phosphate sealing, laser glazing, and sol-gel impregnation were studied as potential methods for increasing the hot-corrosion and erosion resistance of TTBCs. Some microstructural modifications also were made by introducing segmentation cracks into the coating structures by laser glazing and by using special spraying parameters. These last two methods were studied to increase the strain tolerance of TTBCs. The coating microstructures were characterized by optical microscopy, a scanning electron microscopy (SEM), transmission electron microscopy (TEM), energy dispersive spectroscopy (EDS), and x-ray diffraction (XRD). The effect of sealing procedures on the basic thermal and mechanical properties of the coatings was studied. In addition, some correlations between the coating properties and microstructures are also presented, and the advantages and drawbacks of each modification procedure are discussed.

Keywords: diesel engine, hot corrosion, laser glazing, sealing, thermal barrier coating

1. Introduction

1.1 Background of Thermal Barrier Coatings

Thermal barrier coatings (TBCs) are widely used in gas turbine hot-section components such as burners, transition ducts, shrouds, blades, and vanes. The most common TBC material is yttria-stabilized zirconia ($8Y_2O_3$-ZrO_2) due to its high temperature stability, low thermal diffusivity, and high coefficient of thermal expansion (CTE). From the early 1980s, there also have been many investigations into the application of TBCs in diesel engines, but their use is still quite limited. The conditions in the diesel engine combustion chamber differ considerably from those of gas turbine hot sections. Temperatures are lower, but thermal and mechanical loads and hot-corrosion conditions set very demanding requirements for TBCs. Combustion section components of the gas turbine and diesel engine are typically coated by an atmospheric plasma spray (APS) process using coating thicknesses of 200-500 μm. In the first-stage vanes of a gas turbine, the coating thickness is normally in the range of 250-500 μm, and in the combustion chamber component the coating thickness can even be 500-1000 μm. In rotating parts, such as blades, the coating thickness is limited to 125-380 μm by weight and aerodynamic considerations.[1] The large-scale industrial use of thick TBCs (TTBCs; i.e., >1 mm) is still rather limited. However, Nelson and Orenstein[2] reported that TTBCs of 0.75 and 1.1 mm thickness showed less spalling than thinner coatings after 6000 h service in gas turbine combustor liners.

S. Ahmaniemi, J. Tuominen, M. Vippola, P. Vuoristo, and **T. Mäntylä,** Tampere University of Technology/Institute of Materials Science, Tampere, Finland; **F. Cernuschi,** Centro Elettrotecnico Sperimentale Italiano, Segrate, Italy; **C. Gualco,** and **A. Bonadei,** Ansaldo Ricerche, Genova, Italy; and **R. Di Maggio,** University of Trento/Department of Materials Engineering, Trento, Italy; **S. Ahmaniemi** is now at Metso Paper Inc., Global Service Operations, P.O. Box 587, 40101 Jyväskylä, Finland. Contact e-mail: samppa.ahmaniemi@metso.com.

1.2 Demand for Thicker TBCs

Increasing the turbine hot gas inlet temperature (TIT) is a potential way to improve the efficiency of a gas turbine. At the moment, in land-based gas turbines the maximum TIT is around 1500 °C, and in aero engines it is even higher. Since the structural materials, nickel- and cobalt-based superalloys, cannot face temperatures higher than 950 °C, TBCs with better insulation properties are needed. The surface temperatures of the gas turbine hot-section components are mainly controlled by different cooling techniques and TBCs. Although the component air cooling is necessary, the cooling air is taken directly from the compressor, which lowers the output that is available for combustion. Calculations have shown that the temperature drop through the traditional 500 μm TTBC is approximately of 150 °C, but is 320 °C in the case of a 1.8 mm TTBC (if the coating surface temperature is 1250 °C).[3]

With thicker TBCs, the mean combustion temperature of the diesel process also can be increased. This increased temperature does not directly affect the efficiency of the diesel process, but

this extra heat can be recovered in a turbocharger or flue gas boiler in a combined cycle. Some studies have shown that TBCs can increase the coefficient of thermal efficiency of the diesel process or lower the fuel consumption.[4,5] There also have been some positive results concerning the reduction of emissions when using TBCs in diesel engines.[6,7] Without question, the diesel process has to be adjusted correctly to use the benefits of the TBC. Even TTBCs up to 2.5 mm thick have been studied for diesel engine applications.[8]

1.3 Drawbacks of TTBCs

The failure mechanisms that cause TTBC spallation differ to some degree from those of the traditional thin TBCs. A major reason for traditional TBC failure and coating spallation in the gas turbine is typically bond coat oxidation. When the thickness of the thermally grown oxide (TGO) exceeds a certain limit, it induces the critical stress needed for coating failure.[9,10] Besides, during the operation TBCs are exposed to various thermal, mechanical, and chemical loads such as thermal cycling, high- and low-cycle fatigue, high-temperature erosion, and hot corrosion. As mentioned earlier, the risk of the coating failure is higher when increasing the coating thickness. The use of thicker coatings generally leads to higher coating surface temperatures. This can be detrimental if certain limits are exceeded. The long-term phase stability of yttria-stabilized zirconia ($8Y_2O_3$-ZrO_2) deteriorates above 1250 °C. With a thicker coating, the temperature drop through the coating is greater (the dimensional mismatch of the coating surface and bond coat interface region is higher as well). This increases the total strain energy in the structure that is available for crack initiation and growth. In addition, the strain tolerance of a thick coating can be reduced rapidly by sintering effects, if too high a surface temperature is allowed.[11] Even if the CTE of $8Y_2O_3$-ZrO_2 is close to that of the substrate material, the CTE difference between the substrate and coating induces stresses at high temperatures at the coating/bond-coat interface.

1.4 State-of-the-Art TTBC Structures

To overcome the previous problems with TTBCs, much research has been carried out. In practice, the problems have been approached in the following different ways.

- The coating microstructures can be controlled by spray parameters, including temperature control of the substrate and the coating during the deposition. If the system heats up too much during spraying, compressive stresses will develop in the coating structure. For that reason, active substrate and surface cooling are normally used during spraying. Spray parameters also can be adjusted to obtain the desired level of porosity and microcracks. Vertical segmentation crack density in TTBCs can be affected for example by introducing rather thick spray passes,[12] using short spray distance and substrate preheating. In addition to strain tolerance, pores and especially horizontal cracks are naturally advantageous in lowering the thermal conductivity of the coating.
- Extremely high porosity values (up to 25 vol.%) for TBCs have been obtained by spraying polymers together with zirconia.[3] When increasing the coating porosity, the thermal conductivity decreases and Young's modulus is expected to decrease too. However, when spraying polymers together with zirconia the deposition efficiency may decrease to some degree.
- Various gradient and layered structures have been studied to improve the coating properties and to lower the critical stresses caused by the different CTEs of coating and substrate materials.[13,14]
- Several attempts have been made to modify the properties of the TBCs by various post-treatment processes. The coating surface has been modified by liquid metal impregnation,[15] laser glazing,[16-20] hybrid spray processing,[21] solar furnace heat treatment,[22] hot isostatic pressing (HIP),[23,24] sol-gel sealing,[25-27] and phosphate impregnation,[28,29] or by the use of thin chemical vapor deposition (CVD) overlay coatings.[30] When modifying the TBC structures, one should remember that the primary functions of the coating, such as thermal insulation and strain tolerance, should not be deteriorated.

In this article, the microstructures of various modified zirconia-based TTBC structures are characterized extensively. Surface-sealing treatments, such as aluminum phosphate sealing, laser glazing, and sol-gel impregnation, were applied to seal and strengthen the coating surface as well as to introduce segmentation cracks into the coating structure. Here, the authors concentrate mainly on presenting the results of the microstructural characterization of the modified TTBCs, and the mechanical and thermal properties of coatings are briefly discussed. Details regarding the mechanical, thermal, and thermal cycling properties of these coatings can be found in several other studies.[31-33]

2. Experimental

2.1 Preparation of Reference Coatings

Reference $8Y_2O_3$-ZrO_2 coatings were air plasma-sprayed using the Plasma-Technik A3000S system with F4 gun (Sulzer Metco AG, Wohlen, Switzerland) using the Metco 204NS powder. Coatings were sprayed on cleaned and grit-blasted AISI 4142 steel substrates. Afterward, a set of the reference coatings were used in laser glazing, aluminum phosphate impregnation, and sol-gel-sealing experiments. The targeted coating thickness was 1.0 mm. Freestanding coating specimens for thermal property determination purposes and for mercury porosimetry (MP) studies were etched from the substrates using a $50HCl/50H_2O$ solution.

2.2 Aluminum Phosphate Impregnation

Coating surfaces were sealed with an $Al(OH)_3$-$(85\%)H_3PO_4$ solution diluted with 20 wt.% deionized water. The $Al(OH)_3$:$(85\%)H_3PO_4$ ratio was 1:4.2 by weight, which corresponds to the molar ratio P/Al of about 3. The solution was mixed and slightly heated with a magnetic stirrer until it became clear. The freestanding coatings were sealed after detaching from the substrates. Finally, a heat treatment was performed at 300 °C for 4 h.

2.3 Laser-Glazing

Coatings were laser glazed using a 4 kW continuous-wave, fiber-coupled HAAS HL4006D lamp-pumped Nd-YAG laser (HAAS-Laser GmbH, Schramberg, Germany). The width of the laser beam was 10 mm at the focused area, and three parallel 10 mm wide tracks, with 2 mm overlapping, were used to glaze the whole surface of the specimen. More detailed laser-glazing parameters can be found in two other studies.[28,29]

2.4 Sol-Gel Sealing

In sol-gel sealing, the targeted reaction product of the starting materials was ceria-stabilized zirconia ($18CeO_2$-ZrO_2). Starting materials zirconium (IV)-propoxide (70 wt.% solution in 1-propanol) and cerium (III) acetylacetonate hydrate were mixed with solvents (*n*-propyl alcohol and 2-propanol) for 4 h with magnetic stirring without heating. After this time, almost all of the hydrate was dissolved. The dynamic viscosity of the precursor then was fixed in the range of 3.3-3.5 mPa by mixing it with an additive solvent. The precursor was spread on the coatings as droplets from a pipette. After applying the sealant, the specimens were heat treated at 120 °C for 2 h. The sealing and heating cycle was repeated three times to increase the amount of sealant that penetrated into the coating.

2.5 Preparation of the Segmentation-Cracked Coatings

Segmentation-cracked TTBCs were air plasma-sprayed using a V4 plasma gun (SNMI, Avignon, France). Coatings were sprayed on AISI 304 substrates (Ø = 25.4 mm, h = 5 mm) using H.C. Starck's Amperit (Laufenburg, Germany) 827.090 powder. The targeted coating thickness was 1.0 mm, and SICOAT 2453, sprayed using a Diamond Jet Hybrid 2600 HVOF gun (Sulzer Metco AG), was used as a bond coat. Segmentation cracks were introduced to the coatings by applying the coating with quite a high deposition rate (30 μm per pass), a short spray distance (90 mm), and an optimized spray gun velocity (38 m/min). The other main spray parameters were: Ar/H_2 = 35/12 L/min; I = 600 A; U = 67.4 V; and powder feed rate = 55 g/min.

2.6 Characterization

Polished microsections and fracture surfaces were prepared for microscopy analysis. The coating microstructure was analyzed with an optical microscope (Leitz, Wetzlar, Germany), a scanning electron microscope (SEM; model XL-30, Philips, Eindhoven, The Netherlands), and transmission electron microscope (TEM; model JEM 2010, Jeol, Tokyo, Japan). In TEM studies, selected area electron diffraction (SAED) was used to study the crystal structures. Coating-phase structures were characterized by image plate x-ray diffraction (XRD; Italstructures, Riva del Garda, Italy) using filtered CuKα radiation, with the diffractometer operating at 40 kV and 30 mA. The exposure time was 2 h, and the spectrum analyzed was in the 2θ range of 20-120°. The incident angle (Ω) between the x-ray source and the specimen surface was 15°. XRD analysis for the phosphate-sealed coatings was performed after grinding a layer of approximately 50 μm from the surface, because the reaction products of the sealant on the coating surface normally differ considerably from those below the surface. Structural quantitative analyses using XRD patterns were made by the Rietveld method[34] using MAUD software (Material Analysis Using Diffraction, version 1.87, Luca Lutterotti, University of Trento, Italy). Total porosity was evaluated by image analysis (IA) using an Axiophot optical microscope (Carl Zeiss, Wetzlar, Germany) and image acquisition and analysis software (QWin, Leica Microsystems, Heerbrugg, Switzerland). The results and their deviations are presented as a mean value of five separate analyses. Open porosity was measured with MP (models Pascal 140 and Porosimeter 2000, CE-instruments, Milan, Italy) in pressure range of 0.1 kPa to 200 MPa.

2.7 Thermal Properties

Thermal diffusivity $\alpha(T)$ measurements were carried out with the laser flash apparatus Theta (Theta Industries Inc., Port Washington, NY) under vacuum and in the temperature range of room temperature (RT) to 1250 °C. Prior to evaluating the thermal diffusivity, a thin layer of colloidal graphite was painted on both the front and the rear faces to make the sample surfaces opaque. The measurement cycle was repeated three times for each coating to determine the influence of irreversible structural changes. Specific heat measurements, $C_P(T)$, were performed with a differential scanning calorimeter (DSC 404 C, Netzsch-Gerätebau GmbH, Selb, Germany) in the same temperature range, but in air with a scanning rate of 15 °C/min. Specific heat measurements were repeated twice. Alumina crucibles were used in all measurements. Sapphire samples were used as the differential scanning calorimetry (DSC) standards. Thermal conductivities, $k(T)$, were calculated using the equation $k(T) = \alpha(T)*C_P(T)*\rho$, where ρ was the bulk density of the coating. Thermal expansion studies were carried out by dilatometer (model DI-24, Adamel Lhomargy, Paris, France) in air 50-1300 °C. The temperature ramping rate varied from 5-10 °C/min, and the dwell times at maximum temperature ranged from 5 min to 5 h.

2.8 Mechanical Properties

The mechanical properties of the coatings were studied by microhardness measurements and erosion tests. Coatings were tested in the as-sprayed, laser-glazed, and phosphate-sealed state. Coating microhardness ($HV_{0.3}$) was determined with a microhardness tester (Shimadzu, Kyoto, Japan) on the coating cross section, at a position 50 μm from the coating surface. The results are presented as the mean values of the five separate measurements. Erosion tests were performed with a centrifugal accelerator using SiO_2 erosive with a particle size of 0.05-0.1 mm. Specimens were tangentially attached to the centrifuge rim with fixed angles of 90°, 60°, and 30°. The total amount of the erosive was 1 kg, and the average particle velocity was 80 m/s. Residual stresses were measured using the XStress3000 stress analyzer (Stresstech Oy, Vaajakoski, Finland). CrKα radiation was applied at 30 kV and 5.0 mA, with a 30 s exposure time. The traditional $\sin^2\psi$ method was carried out using specimen tilts of ψ = ±0°, ±21.8°, ±31.7°, and ±40°. The peak shifts of zirconia coatings were studied on (3 1 3) crystalline plane of t'-ZrO_2 at a 2θ position of 153°. Bulk material constants E = 205 GPa and ν = 0.23 for zirconia were used in the stress calculations. Through-thickness stress profiles were determined by repeating the mea-

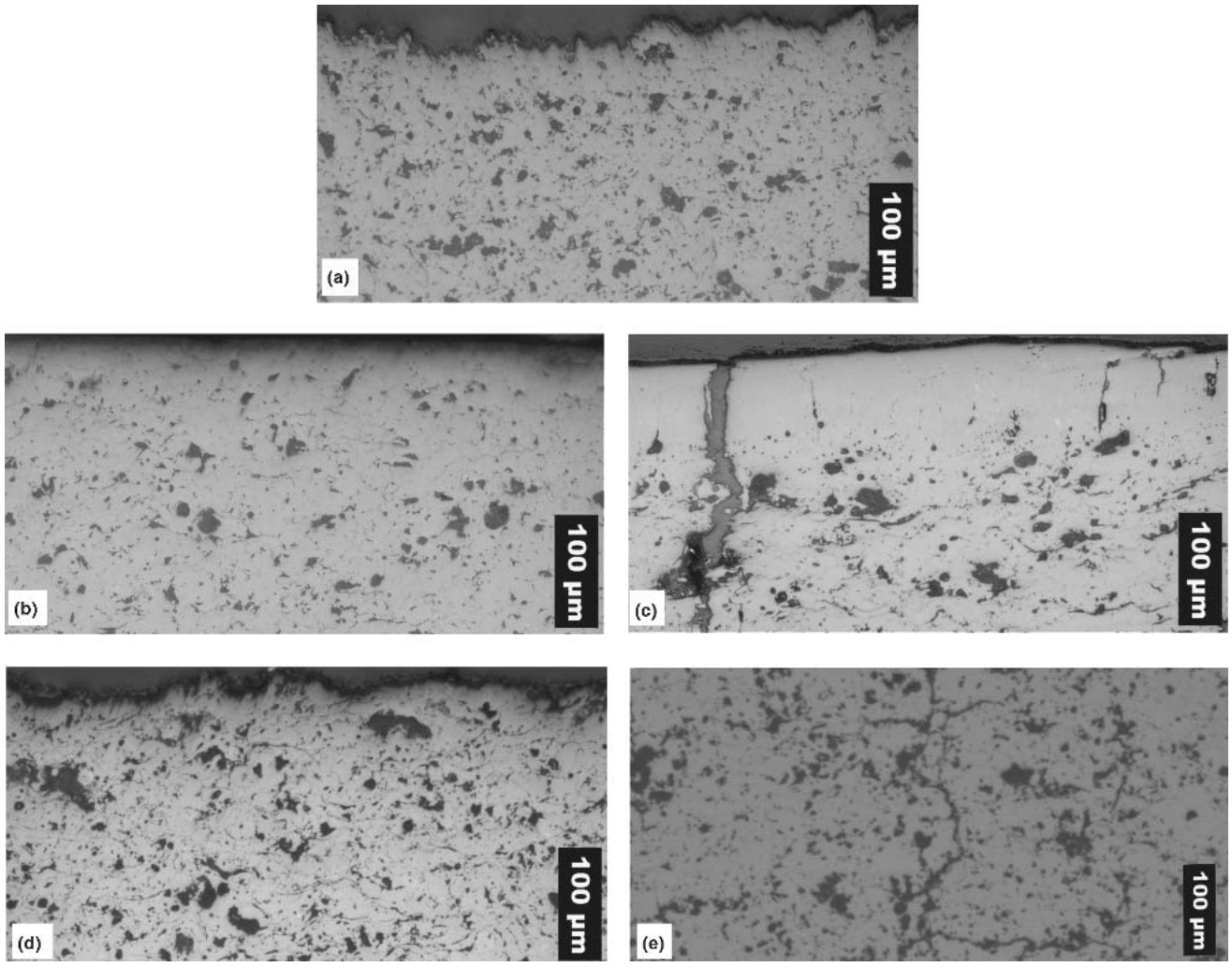

Fig. 1 Optical micrographs of the $8Y_2O_3$-ZrO_2 coatings: **(a)** reference coating; **(b)** aluminum phosphate sealed coating; **(c)** laser-glazed coating; **(d)** sol-gel-sealed coating; and **(e)** segmentation-cracked coating

surements and the layer removal steps. Layers were removed with careful grinding to avoid additional stresses or cracks.

3. Results

3.1 Microstructural Characterization

Optical micrographs of all modified $8Y_2O_3$-ZrO_2 coatings are presented in Fig. 1. In the reference coating, the typical microstructure of the plasma-sprayed TBCs could be seen along with pores, lamellae boundaries, and microcracks. Optical micrographs showed the characteristic microstructures of all the modified coatings. The densification effect of aluminum phosphate sealing and laser glazing could be seen as well as the crack structures in laser-glazed and segmentation-cracked coatings. However, in optical microscopy studies of the sol-gel-sealed coatings no effect of the impregnation procedure was observed.

The total porosities of the coatings were evaluated by IA from the polished cross section of the coating. The sealed coatings were only analyzed in the region of the sealed top layers. The measurements of total and open porosity are presented in Table 1. Total porosity was significantly reduced by aluminum phosphate sealing (39%) and especially by laser glazing (86%). Sol-gel sealing reduced the total porosity only slightly (15%). The total porosity of the segmentation-cracked coating was rather low (12.7%) and was probably a consequence of the short spray distance. Open porosity measurements were carried out by MP and showed approximately the same relative porosity reduction as that of aluminum phosphate sealing (43%). The pore size distribution of open porosity varied in the range of 0.006-10 μm, and the major fraction of the pores was found at 0.1-0.5 μm. The determination of total porosity by IA was very sensitive to the specimen preparation procedure. Normally, the evaluated total porosity values are too high because in specimen preparation some defects, namely pullouts, can be introduced and identified as pores. So for that reason the real total porosity could be expected to be somewhere between the values measured by IA and MP

3.1.1 Aluminum Phosphate Sealed Coatings. Optical microscopy studies showed that the aluminum phosphate sealant

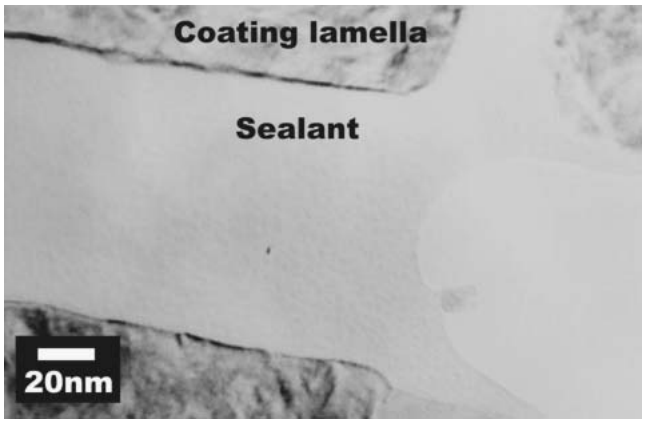

Fig. 2 TEM micrograph of the aluminum phosphate sealed $8Y_2O_3$-ZrO_2 coatings showing the sealant penetrating into the coating crack

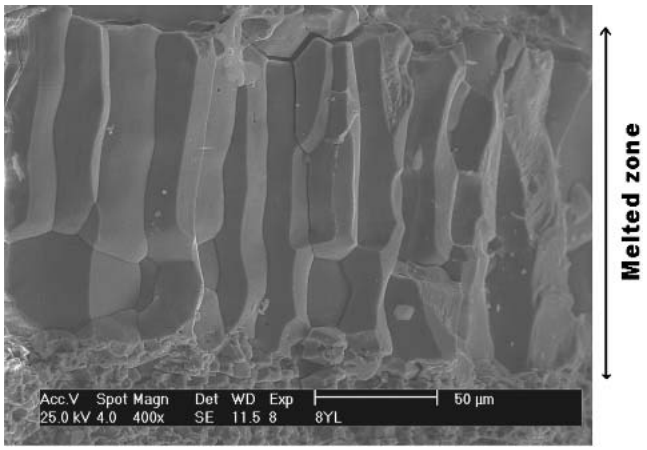

Fig. 3 Vertically oriented columnar grains in an SEM micrograph of the laser-glazed $8Y_2O_3$-ZrO_2 coating

Table 1 Basic Properties of Modified $8Y_2O_3$-ZrO_2 Coatings

Coating	Coating Thickness, mm	Thickness of the Sealed Layer, µm	Macrocrack Density, 1/mm	Microhardness, $HV_{0.3}$	Total Porosity, vol.% (image analysis)	Open Porosity, vol.% (mercury porosimetry)
8YSZ reference	1.0	…	…	604	20.7 ± 1.8	9.3 ± 1.0
8YSZ AP sealed	1.0	300-400	…	949	12.6 ± 1.9(a)	5.3 ± 1.0
8YSZ laser	1.0	100-150	1.5	1240	2.8 ± 2.6(a)	Not measured
8YSZ sol-gel	1.0	Through thickness	…	698	17.5 ± 1.7(a)	Not measured
8YSZ segment	1.0	…	1.2	Not measured	12.7 ± 1.9	Not measured

(a) Measured from the top layer of the cross section

penetrated 300-400 µm into the coatings. As mentioned earlier, the porosity of the coating was decreased by approximately 40% due to the sealing. XRD studies did not show traces of crystalline sealant phases or reaction products in the coating structure. An example of the sample with a sealant, properly penetrated into the interlamellar spacing of the coating, is shown in the TEM micrograph in Fig. 2.

In contrast to the results of the authors' earlier study[35] of phosphate-sealed alumina coatings, no indication of a reaction layer was found at the interface of the sealant/coating lamella. Ring patterns in the SAED analyses, which were taken from the penetrated sealant, confirmed the amorphous structure of the sealant. The sealing heat treatment was performed at 300 °C, and the crystalline phosphate phases were expected to occur at much higher temperatures. More detailed studies of the aluminum phosphate sealed zirconia coatings can be found in two other studies.[28,29]

3.1.2 Laser-Glazed Coatings. In the laser-glazed coating, the melted region was highly densified, but some vertical cracks were detected especially in the melted zone. The depth of the melted layer was 80-120 µm, indicating that the melting was quite uniform. SEM studies showed that in some places the melted zone consisted of two variant layers. The uppermost layer was formed of pentagonal and hexagonal plates, and the underneath layer of columnar grains. The columnar grain structure is shown in the fracture surface of the laser-glazed coating (Fig. 3). Two types of vertical cracks were detected in the laser-glazed coating. Within the melted layer, there were some vertical microcracks with lengths that were shorter than the layer thickness. There were also some longer macrocracks, 200-500 µm in length, which went down through the glazed layer and further. These macrocracks were rather straight lines in the vertical direction, and their density was rather close to that in the segmentation-cracked coatings (Table 1). More results of the laser-glazed TBC coatings can be found in other studies.[28,29]

3.1.3 Sol-Gel-Sealed Coatings. SEM micrographs of the sol-gel-sealed coating are presented in Fig. 4. In optical micrographs, the sealing effect was not seen as a decreased porosity. For improving the sealant impregnability, and especially for preventing the premature gelling of the sealant on the coating surface, the solvent content was fixed to a rather high level. For that reason, the molecular concentration of the precursor was low, and a strong evaporation of the solvent during the heat treatment (at 120 °C) occurred. As a consequence of that, the solid matter content, which originated from the sealant, remained quite small. The extra sealant on the coating surface was easily detected in SEM studies, marked with an arrow in Fig. 4(a). Also some remains of the penetrated sealant in the open pores of the coating could be observed in backscatter electron image (marked with an arrow in Fig. 4b). These cerium-rich regions were detected also in the EDS point analyses.

3.1.4 Segmentation-Cracked Coatings. In the segmentation-cracked coatings, two types of cracks existed. Vertical segmentation cracks were rather long (100-500 µm), but horizontally oriented branching cracks were much shorter (50-200 µm). The length of the segmentation cracks was approximately equal to the length of the vertical macrocracks in the laser-glazed coatings. As mentioned earlier, the crack densities were also

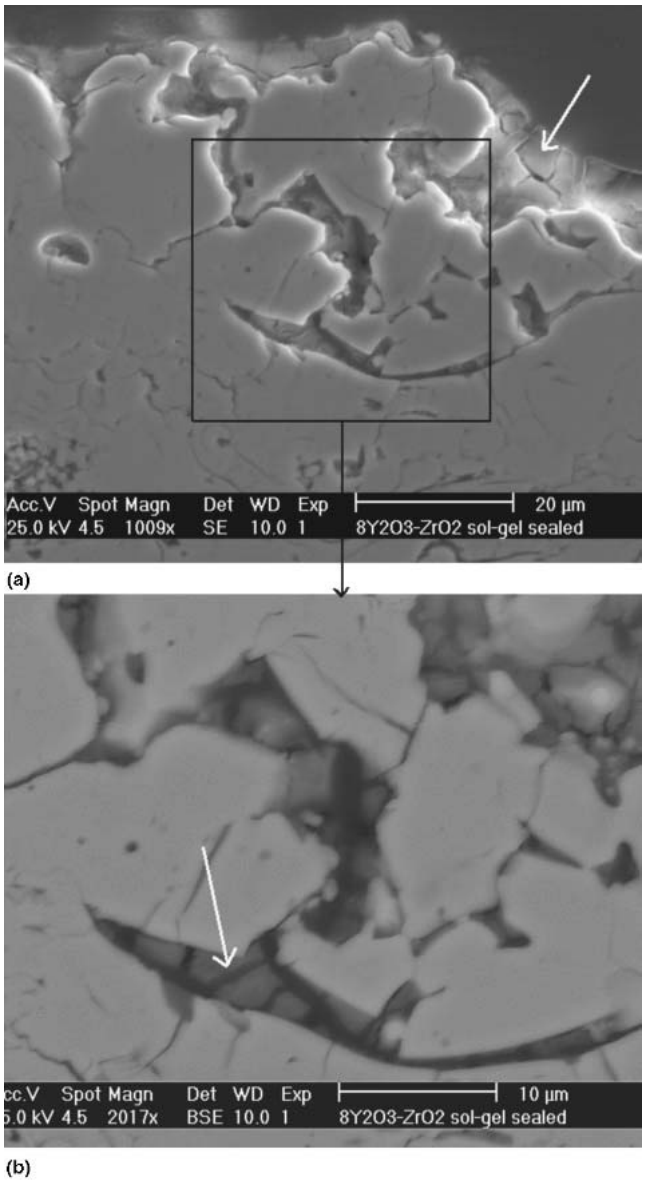

Fig. 4 SEM micrographs of the sol-gel-sealed $8Y_2O_3$-ZrO_2 coating: **(a)** secondary electron image; and **(b)** backscatter electron image. Solid matter, originating from the sealant, is indicated by the white arrows.

fairly similar. However, in the segmentation-cracked coatings the cracks were more randomly located over the whole coating thickness, whereas in the laser-glazed coating the cracks were situated near the coating surface. Overview micrographs of the segmentation-cracked and laser-glazed coatings are presented in Fig. 5. In the study by Ahmaniemi et al.,[32] it was shown that both segmentation-cracked and laser-glazed coatings have excellent thermal cycling resistance compared with that of normal TTBCs.

3.2 Thermal Properties

Thermal diffusivity, $\alpha(T)$, specific heat, $C_P(T)$, and thermal expansion, $[dl/l_o](T)$, were determined as a function of temperature from 100-1300 °C. For each specimen, the measurements were repeated to discover the temperature-dependent structural changes. In some cases, measurements also were made for heat-treated coatings (5 h at 1250 °C in air).

Thermal conductivities, $k(T)$, were calculated using the equation $k(T) = \alpha(T)*C_P(T)*\rho$, where ρ was the density of the coating. Thermal conductivity results are presented in Fig. 6. In the case of reference coating, the effect of splat boundary sintering, during the first measurement cycle could be seen clearly as an increase of $k(T)$ values in the second cycle. However, the increase in thermal conductivity was more emphasized at temperatures below 1000 °C. The $\alpha(T)$ data showed during the first measurement cycle that sintering started to appear around 1000 °C. Zhu and Miller[11] demonstrated by isothermal k measurements at 990, 1100, and 1320 °C that the major increase in k takes place during the first 5-10 h. The thermal conductivity of the laser-glazed coatings was almost the same as that of the as-sprayed coatings. That was reasonable because only a relatively thin surface layer (80-120 µm) of the total coating thickness (1.0 mm) was densified. Instead, the aluminum phosphate sealing clearly increased the $k(T)$ values of the coating. The $\alpha(T)$ values of the phosphate-sealed coating were high compared with the as-sprayed coating, and the values were almost doubled over the whole temperature range. The sealant penetration into the interlamellar cracks, which was seen in the TEM micrographs, can explain the higher $\alpha(T)$ values. The sealant in the cracks and pores had acted as a thermal diffusion bridge through the coating structure. In fact, the $\alpha(T)$ of the sealant had to be higher than that of zirconia, because the $k(T)$ of the phosphate-sealed coating was even higher than that of bulk yttria-stabilized zirconia.

In the first cycle of the C_P measurement, there was an exothermic peak at 200-600 °C and an endothermic peak at 950-1000 °C in the aluminum phosphate sealed coating. These peaks also can be seen in the $k(T)$ data in Fig. 6. The exothermic peak at low temperature was probably a consequence of the reactions of the aluminum phosphate sealant or were caused by the crystallization of the amorphous sealant phase. These were not finished during the sealing treatment (4 h at 300 °C). The endothermic peak at high temperature is more difficult to interpret, but it could have been caused by the structural change of the aluminum phosphate. As the peaks were not present in the second measurement cycle, the changes were not reversible.

The sintering effect was also found in the thermal expansion study as a densification of the as-sprayed reference coatings. Densification started to take place at around 1000 °C (Fig. 7). The effect of the temperature ramping rate (5 or 10 °C/min) could not be seen in the thermal expansion curves, but the influence of the dwell time (5 min or 5 h) at maximum temperature could clearly be observed. In the heat-treated specimen (1250 °C, 5 h) only a very limited increase in density was detected.

The structural anisotropy in the coating should be taken into account in the interpretation of the effect of sintering on the basis of thermal conductivity and thermal expansion results. Thermal conductivity was determined in the perpendicular direction to the coating surface, but thermal expansion was determined in longitudinal direction.

In the case of aluminum phosphate sealed coating, sintering was probably hindered a bit by the sealant (Fig. 8). Instead of

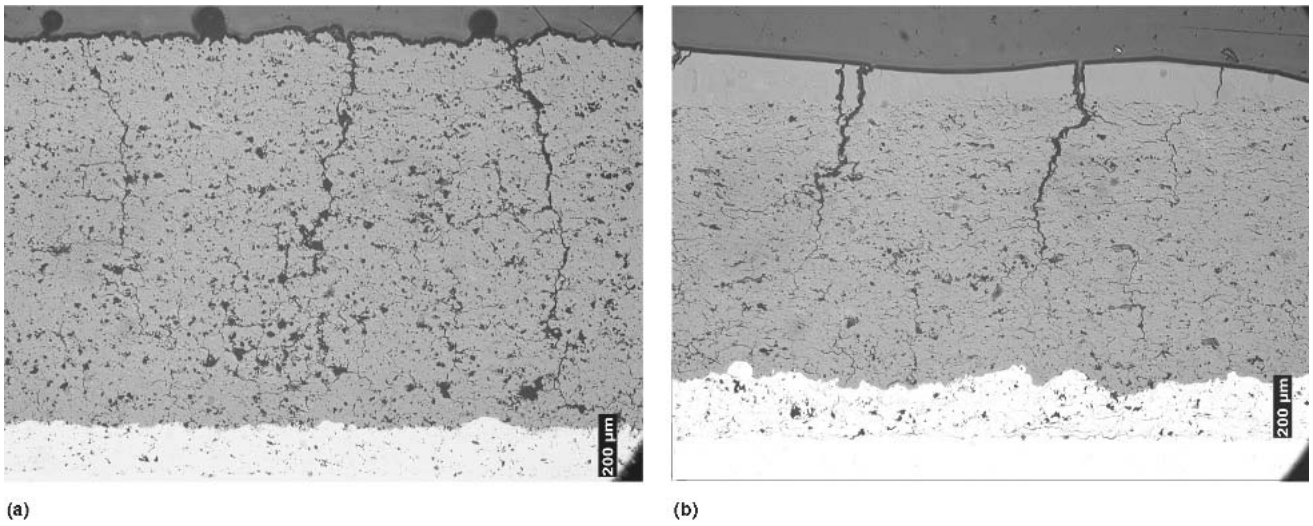

Fig. 5 Optical micrographs of the **(a)** segmentation-cracked $8Y_2O_3$-ZrO_2 coating and **(b)** laser-glazed $8Y_2O_3$-ZrO_2 coating.[33] The micrographs were taken after the thermal cycling tests.

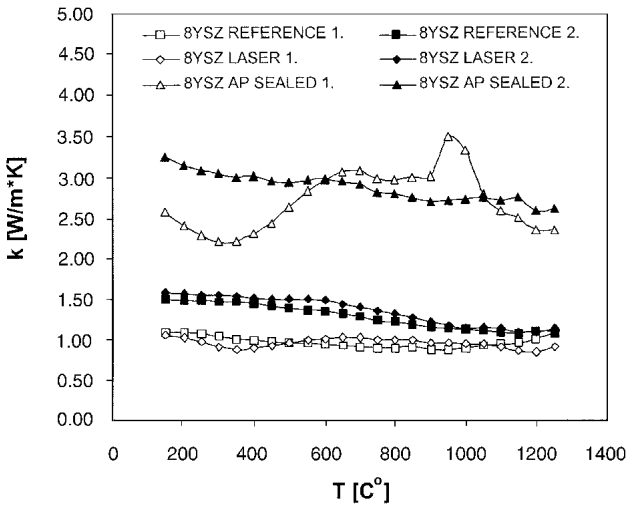

Fig. 6 Thermal conductivity of some modified coatings as a function of temperature: 1 = first measurement cycle; 2 = second measurement cycle

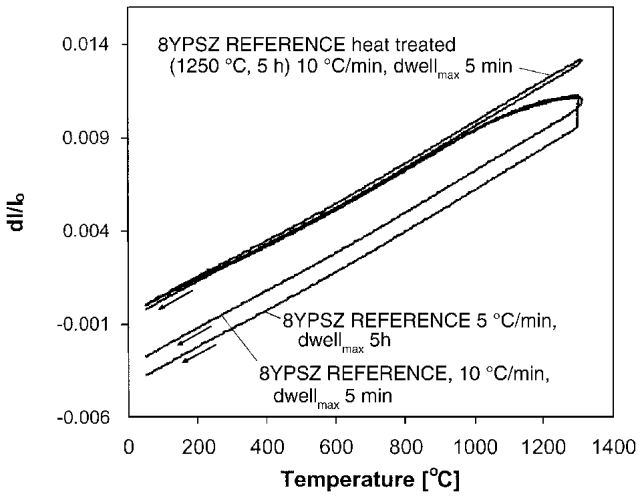

Fig. 7 Thermal expansion curves for the reference $8Y_2O_3$-ZrO_2 coatings as a function of temperature

sintering, some other structural changes had taken place. This could be seen as a nonlinear irreversible thermal expansion curve of the heat-treated specimen (1250 °C, 5 h). XRD studies of the aluminum phosphate sealed coating showed that the phase structure of zirconia (t'-ZrO_2) was destabilized to a certain degree (40 vol.% m-ZrO_2) after the measurement run. At high temperatures, 1000-1300 °C, the t'-ZrO_2 structure had partially destabilized, but the tetragonal phase did not change to monoclinic due to the high temperature. When coming down from high temperatures, the phase change (t-$ZrO_2 \rightarrow m$-ZrO_2), accompanied by a volume increase, had started to take place at 600 °C and continued down to 200 °C. The phase changes were more apparent in the heat-treated specimen, and the m-$ZrO_2 \rightarrow t$-ZrO_2 phase change also could be seen in the temperature region of 300-1000 °C in the heating curve. An aluminum phosphate sealed coating heated up to 980 °C did not show any phase changes, and the ascending and descending curves were almost linear. The thermal properties of these coatings are presented in more detail in the article by Ahmaniemi et al.[32]

3.3 Mechanical Properties

Microhardness results are presented in Table 1 as $HV_{0.3}$ values. All the sealing treatments increased the microhardness of the reference coating. By laser glazing, the hardness values were even doubled. Aluminum phosphate sealing increased the hardness by 57%, and sol-gel sealing by 16%.

The erosion resistances of the aluminum phosphate sealed and laser-glazed $8Y_2O_3$-ZrO_2 coatings were much higher when compared with that of the as-sprayed reference coating (Fig. 9). The wear volumes of the aluminum phosphate sealed coatings were low, and the erosion resistance was improved by approxi-

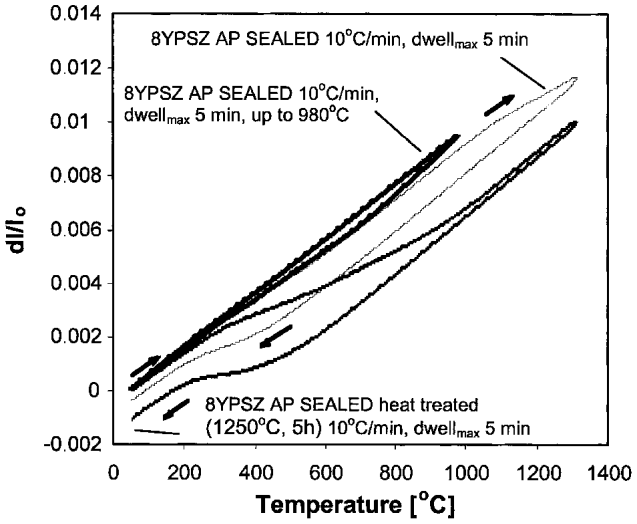

Fig. 8 Thermal expansion curves for the aluminum phosphate sealed $8Y_2O_3$-ZrO_2 coatings as a function of temperature

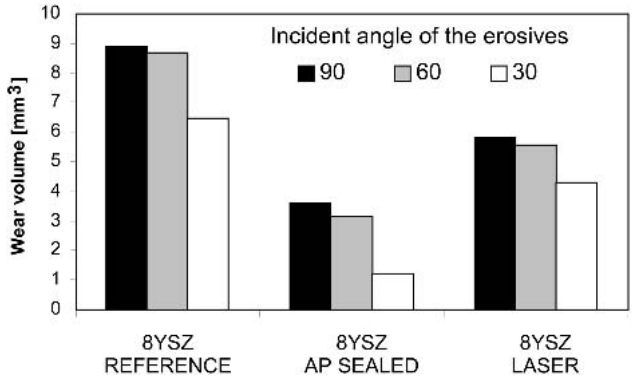

Fig. 9 Erosion wear volumes of the $8Y_2O_3$-ZrO_2 coatings as a function of different incident angles

mately 67%. In the case of the laser-glazed coating, the improvement was 33%. The melted layer of the laser-glazed coating was worn out locally, so at the end of the experiment there were some as-sprayed surface areas that were susceptible to the erosives.

Residual stress analyses, profiled through the coating thickness, showed only a slight tensile stress state in the reference coating. Instead of that, a strong compressive stress state at the surface of the aluminum phosphate sealed coating was detected (Fig. 10). The compressive stresses could be found only in the uppermost layer of the coating, and they were obviously linked to the penetration depth of the sealant. Compressive stresses, and their origins in plasma-sprayed alumina and chromia coatings caused by phosphate sealing, are discussed in more detail in the authors' earlier study.[36] The measurement accuracy of the laser-glazed coating was rather poor, due to the columnar crystal orientation and the large grain size of the melt layer. That explains the strong variation of the results near the coating surface. However, at sufficient depth from the surface (~350 μm) the stresses were almost equal in all coatings. A more detailed study of mechanical properties of these coatings is presented in the article by Ahmaniemi et al.[31]

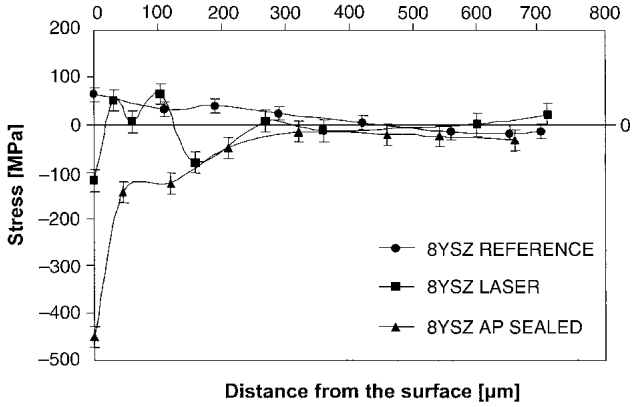

Fig. 10 Residual stress profiles of the $8Y_2O_3$-ZrO_2 coatings

4. Summary and Conclusions

In this article, several modified $8Y_2O_3$-ZrO_2-based TTBC structures were introduced and characterized. Their microstructures were discussed, and some results concerning their mechanical and thermal properties were presented. With respect to the advantages and drawbacks of each modification procedure, the following conclusions could be made:

- Characterization results showed that aluminum phosphate sealing is a very effective strengthening method for TTBCs. The sealing treatment reduced the coating porosity and increased the microhardness and erosion resistance significantly. This effective sealing method could also be beneficial in improving the hot corrosion behavior of TTBCs. However, the aluminum phosphate sealing increased the thermal conductivity of the coating significantly, and the phase structure of the sealed coating was not stable above 1000 °C. In addition, a dense microstructure with high compressive stresses might be disadvantageous for the coating when exposed to high thermal loads. Therefore, aluminum phosphate sealed $8Y_2O_3$-ZrO_2 should not be used above 1000 °C.
- The surface layer of the laser-glazed coating was very dense and contained a certain amount of vertical micro- and macrocracks. The thermal properties of the laser-glazed coating were close to those of the as-sprayed reference coating, but the wear and erosion properties were significantly improved. The vertical crack network in the laser-glazed coating was rather similar to the one in the segmentation-cracked coating. So for that reason the laser-glazed structure could be expected to have a good strain tolerance.
- The microstructure of the $8Y_2O_3$-ZrO_2 did not change a lot due to the sol-gel sealing, even when the procedure was applied three times. Effective sealing was prevented by the strong evaporation of the solvent, and for that reason the solid matter content, which originated in the sealant and was left in the coating pores and cracks, was quite low. However, the sealant composition could be further developed to avoid this problem.
- In the segmentation-cracked coating, the crack structure and orientation in the coating was controlled by the spray

parameters. Segmentation cracks were introduced by thick spray passes, a short spray distance, and certain surface velocities. Even if the segmentation-cracked coatings have a good strain tolerance, their erosion and hot corrosion resistance may slightly deteriorate because of the vertical and horizontal cracks.

Additional work is still required for a better understanding of the high-temperature properties of the modified TTBCs. For that reason, future work will include comprehensive studies of hot corrosion and thermal cycling.

Acknowledgments

Results in this study have been collected from the work carried out in COST522 Work Package 2 Protective Systems at Tampere University of Technology (Finland), CESI (Italy), and Ansaldo (Italy) during the years 2001 and 2002. Sol-gel-related studies were mainly performed at the University of Trento (Italy). All the authors are grateful to their national financial supporters.

References

1. W.P. Parks, E.E. Hoffman, W.Y. Lee, and I.G. Wright: "Thermal Barrier Coatings Issues in Advanced Land-Based Gas Turbines," *J. Thermal Spray Technol.,* 1997, *6*(2), pp. 187-92.
2. W.A. Nelson and R.M. Orenstein: "TBC Experience in Land-Based Gas Turbines," *J. Thermal Spray Technol.,* 1997, *6*(2), pp. 176-80.
3. C. Gualco, E. Cordano, F. Fignino, C. Gambaro, S. Ahmaniemi, S. Tuurna, T. Mántylá, and P. Vuoristo: "An Improved Deposition Process for Very Thick Porous Thermal Barrier Coatings" in *International Thermal Spray Conference,* E. Lugscheider and C.C. Berndt, ed., DVS Deutscher Verband für Schweißen, Dusseldorf, Germany, 2002, pp. 195-201.
4. D.N. Assanis: "Thin Thermal Barrier Coatings for Internal Combustion Engine Components," *Int. J. Mater. Prod. Technol.,* 1989, *4,* pp. 232-43.
5. K. Osawa, R. Kamo, and E. Valdmanis: "Performance of Thin Thermal Barrier Coating on Small Aluminium Block Diesel Engine," SAE Technical Paper Series, No. 910461, 1991, pp. 1-8.
6. M. Vittal, J.A. Borek, D.A. Marks, A.L. Boehman, D.A. Okrent, and A.P. Bentz: "The Effect of Thermal Barrier Coatings on Diesel Engine Emissions," *Trans. ASME,* 1999, *121,* pp. 218-25.
7. D.W. Parker: "Thermal Barrier Coatings for Gas Turbines, Automotive Engines and Diesel Equipment," *Mater. Design,* 1992, *13*(6), pp. 345-51.
8. R.C. Brink: "Material Property Evaluation of Thick Thermal Barrier Coating Systems," *Trans. ASME,* 1989, *111,* pp. 570-77.
9. J.P. Singh, B.G. Nair, D.P. Renusch, M.P. Sutaria, and M.H. Grimsditch: "Damage Evolution and Stress Analysis in Zirconia Thermal Barrier Coatings During Cyclic and Isothermal Oxidation," *J. Am. Ceram. Soc.,* 2001, *84*(10), pp. 2385-93.
10. A.G. Evans, D.R. Mumm, J.W. Hutchinson, G.H. Meier, and F.S. Pettit: "Mechanisms Controlling the Durability of Thermal Barrier Coatings," *Prog. Mater. Sci.,* 2001, *46,* pp. 505-53.
11. D. Zhu and R.A. Miller: "Thermal Conductivity and Elastic Modulus Evolution of Thermal Barrier Coatings Under High Heat Flux Conditions," *J. Thermal Spray Technol.,* 2000, *9*(2), pp. 175-80.
12. D. Schwingel, R. Taylor, T. Haubold, J. Wigren, and C. Gualeo: "Mechanical and Thermophysical Properties of Thick PYSZ Thermal Barrier Coatings: Correlation with Microstructure and Spraying Parameters," *Surf. Coat. Technol.,* 1998, *108-109,* pp. 99-106.
13. M. Tamura, M. Takahashi, J. Ishii, K. Suzuki, M. Sato, and K. Shimomura: "Multilayered Thermal Barrier Coatings for Land-Base Gas Turbines," *J. Thermal Spray Technol.,* 1999, *8*(1), pp. 68-72.
14. Y. Lee, D.P. Stinton, C.C. Berndt, F.E. Erdogan, Y.D. Lee, and Z. Mutasim: "Concept of Functionally Graded Materials for Advanced Thermal Barrier Coating Applications," *J. Am. Ceram. Soc.,* 1996, *79*(12), pp. 3003-12.
15. A. Ohmori, Z. Zhou, K. Inoue, K. Murakami, and T. Sasaki: "Sealing and Strengthening of Plasma-Sprayed ZrO_2 Coating by Liquid Mn Alloy Penetration Treatment" in *Thermal Spraying: Current Status and Future Trends,* A. Ohmori, ed., High Temperature Society of Japan, Osaka University, Osaka, Japan, 1995, pp. 549-54.
16. I. Zaplatynsky: "Performance of Laser-Glazed Zirconia Thermal Barrier Coatings in Cyclic Oxidation and Corrosion Burner Rig Test," *Thin Solid Films,* 1982, *95,* pp. 275-84.
17. R. Sivakumar and B.L. Mordike: "Laser Melting of Plasma Sprayed Ceramic Coatings," *Surf. Eng.,* 1988, *4*(2), pp. 127-40.
18. K.M. Jasim, D.R.F. West, W.M. Steen, and R.D. Rawlings: "Laser Surface Sealing of Plasma Sprayed Yttria Stabilized Zirconia Ceramics" in *Proceedings of the Laser Materials Processing 1988 Conference,* Springer-Verlag, Heidelberger, Berlin, Germany, 1989, pp. 17-31.
19. H.L. Tsai and P.C. Tsai: "Microstructures and Properties of Laser-glazed Plasma-sprayed ZrO_2-YO1.5/Ni-22Cr-10Al-1Y Thermal Barrier Coatings," *J. Mater. Eng. Perform.,* 1995, *4*(6), pp. 689-96.
20. K.A. Khor and S. Tana: "Pulsed Laser Processing of Plasma Sprayed Thermal Barrier Coatings," *J. Mater. Process. Technol.,* 1997, *66,* pp. 4-8.
21. Z. Zhou, N. Eguchi, H. Shirasawa, and A. Ohmori: "Microstructure and Characterization of Zirconia-Yttria Coatings Formed in Laser and Hybrid Spray Process," *J. Thermal Spray Technol.,* 1999, *8*(3), pp. 405-13.
22. A. Ferriere, L. Lestrade, A. Rouanet, A. Denoirjean, A. Grimaud, and P. Fauchais: "Solar Furnace Surface Treatment of Plasma-Sprayed Thermal Barrier Coatings," *J. Thermal Spray Technol.,* 1994, *3*(4), pp. 362-70.
23. H. Kuribayashi, K. Suganuma, Y. Miyamoto, and M. Koizumi: "Effect of HIP Treatment on Plasma-Sprayed Ceramic Coating onto Stainless Steel," *Am. Ceram. Soc. Bull.,* 1986, *65*(9), pp. 1306-10.
24. K.A. Khor and N.L. Loh: "Hot Isostatic Pressing of Plasma Sprayed Thermal Barrier Coating Systems," *Mater. Manuf. Proc.,* 1995, *10*(6), pp. 1241-56.
25. K. Moriya, W. Zhao, and A. Ohmori: "Improvement of Plasma-Sprayed Ceramic Coatings Treated by Sol-Gel Process" in *Thermal Spraying: Current Status and Future Trends,* A. Ohmori, ed., High Temperature Society of Japan, Osaka University, Osaka, Japan, 1995, pp. 1017-21.
26. G. John and T. Troczynski: "Surface Modification of Thermal Sprayed Coatings" in *Thermal Spray: Practical Solutions for Engineering Problems,* C.C. Berndt, ed., ASM International, Materials Park, OH, 1996, pp. 483-88.
27. T. Troczynski, Q. Yang, and G. John: "Post-Deposition Treatment of Zirconia Thermal Barrier Coatings Using Sol-Gel Alumina," *J. Thermal Spray Technol.,* 1999, *8*(2), pp. 229-34.
28. S. Ahmaniemi, P. Vuoristo, and T. Mäntylä: "Sealing Procedures for Thick Thermal Barrier Coatings," *J. Thermal Spray Technol.,* 2002, *11*(3), pp. 320-32.
29. S. Ahmaniemi, J. Tuominen, P. Vuoristo, and T. Mäntylä: "Improved Sealing Treatments for Thick Thermal Barrier Coatings," *Surf. Coat. Technol.,* 2002, *151-52,* pp. 412-17.
30. V.A.C. Haanappel, J.B.A. Scharenborg, H.D. Corbach, T. Fransen, and P.J. Gellings: "Can Thermal Barrier Coatings Be Sealed by Metal-Organic Chemical Vapour Deposition of Silica and Alumina?," *High Temp. Mater. Proc.,* 1995, *14*(2), pp. 57-66.
31. S. Ahmaniemi, P. Vuoristo, and T. Mäntylä: "Mechanical and Elastic Properties of Modified Thick Thermal Barrier Coatings," *Mater. Sci. Eng. A Struct.,* 2004, *366,*(1), pp. 175-82.
32. S. Ahmaniemi, P. Vuoristo, T. Mäntylä, F. Cernuschi, and L. Lorenzoni: "Modified Thick Thermal Barrier Coatings: Part II. Thermophysical Characterization," *J. Eur. Ceram. Soc.,* 2004, *24,* pp. 2669-79.
33. S. Ahmaniemi, P. Vuoristo, T. Mäntylä, C. Gualco, A. Bonadei, and R. Di Maggio: "Thermal Cycling Resistance of Modified Thick Thermal Barrier Coatings," *Surf. Coat. Technol.* (in press)
34. R.A. Young: *The Rietveld Method,* Oxford University Press, Oxford, UK, 1993.
35. M. Vippola, S. Ahmaniemi, J. Keränen, P. Vuoristo, M. Buchmann, and R. Gadow: "Aluminum Phosphate Sealed Alumina Coating: Characterization of Microstructure," *Mater. Sci. Eng. A Struct.,* 2002, *323,* pp. 1-8.
36. S. Ahmaniemi, M. Vippola, P. Vuoristo, T. Mäntylä, M. Buchmann, and R. Gadow: "Residual Stresses in Aluminium Phosphate Sealed Plasma Sprayed Oxide Coatings and Their Effect on Abrasive Wear," *Wear,* 2002, *252,* pp. 614-23.